# A Numerical Study of "Hijikawa-Arashi": A Thermally Driven Gap Wind Visualized by Nocturnal Fog

JUNSHI ITO

*Atmosphere and Ocean Research Institute, The University of Tokyo, Kashiwa, Chiba, Japan*

TOSHIYUKI NAGOSHI

*Iwate University, Morioka, Iwate, Japan*

HIROSHI NIINO

*Atmosphere and Ocean Research Institute, The University of Tokyo, Kashiwa, Chiba, Japan*

## ABSTRACT

A renowned local wind in Japan, "Hijikawa-Arashi," is a thermally driven nocturnal gap wind accompanied by fog. The wind is visually identified by the fog along the valley of the Hijikawa River between the Ozu basin and the Seto Inland Sea during the early morning in autumn and winter. A fine-resolution numerical model is employed to reproduce the main observed features of Hijikawa-Arashi. A vertical resolution of 10 m or less at the lowest level is required to express the nocturnal radiative cooling of the land that is required for fog formation in the basin, and fine horizontal resolution is necessary to express a realistic valley through which the fog is advected to the sea. Multiple hydraulic jumps accompanied by supercritical flow occur because of the complex topography. Both moisture transport by the sea breeze during the daytime and evaporation from the land surface are important for accumulating moisture to produce the fog.

## 1. Introduction

"Hijikawa-Arashi" is the Japanese name for a stormy wind that blows along the Hijikawa River in Ozu City, Ehime Prefecture, Shikoku Island, Japan (Fig. 1). It is a southeasterly wind that blows from the Ozu basin to the estuary of the Hijikawa River. A unique feature of Hijikawa-Arashi is that it can be observed without instruments because it is fascinatingly visible because of the accompanying radiative fog that develops from the surface in the Ozu basin during a clear night with calm winds (Fig. 2; see supplemental movie S1 in the online

supplemental material and the description therein). It occurs in early morning during late autumn and early winter when the synoptic pressure gradient is weak and the weather is fair, and is most frequent in November. The magnificent scenery of Hijikawa-Arashi is one of the natural tourist attractions in that region, and the local government, Ozu City, maintains a panoramic viewpoint in a park on a hill adjacent to the Hijikawa River (point 2 in Fig. 3a; Fig. 3b).

The topography around the region where Hijikawa-Arashi occurs is quite complex. The Hijikawa River has a number of branches that originate from the westernmost edge of the mountain range on Shikoku Island (Fig. 1c). Many of these branches first flow southward, which is opposite to the final flow direction of the Hijikawa to the Seto Inland Sea in the north.[1] These branches join together in

---

⊙ Denotes content that is immediately available upon publication as open access.

✎ Supplemental information related to this paper is available at the Journals Online website: https://doi.org/10.1175/JAMC-D-18-0189.s1.

*Corresponding author*: Junshi Ito, junshi@aori.u-tokyo.ac.jp

---

[1] In fact, "Hiji" in Japanese means an arm representing an arm bent at the elbow and "Kawa" means river, so that "Hijikawa" means a river with a large bend.
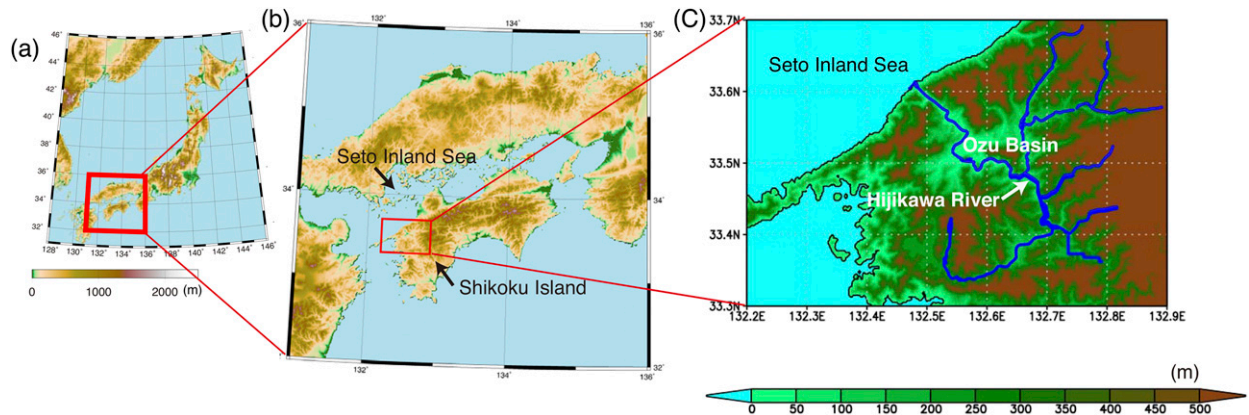
FIG. 1. Topographic maps of (a) Japan, (b) Shikoku Island, and (c) the Ozu basin. The red square in (a) indicates the area shown in (b), and the red rectangle in (b) indicates the area shown in (c). Blue lines in (c) indicate the Hijikawa River and its major branches.

the Ozu basin to form a single final channel of 10-km length, where the river flows out to the Seto Inland Sea through a narrow valley. At its narrowest, the valley is about 100 m wide (Fig. 1c), and the elevation of the valley bottom within the basin is only ~10 m above sea level.

The dynamics of Hijikawa-Arashi do not appear to be the same as those of many other local winds reported in the literature, as discussed by Ohashi et al. (2015). Hijikawa-Arashi may be classified as a type of gap wind, which is defined as a strong low-level wind through a channel or a gap driven by a pressure gradient (see http://glossary.ametsoc.org/wiki/Gap_wind). Mayr et al. (2007) presented a comprehensive review of the dynamics of gap wind, and Ohashi et al. (2015) presented a list of studies of gap winds.

Most gap winds are driven by a pressure gradient that is imposed by a synoptic-scale disturbance. However, in some cases, gap winds are driven by the diurnal thermal contrast between a large plain and a smaller basin or valley that has a lesser heat capacity. These gap winds are likely to reverse their direction during the daytime

and nighttime transitions (e.g., Zängl 2004; Chrust et al. 2013; Finn et al. 2016). For gaps with larger scales, on the other hand, both of the synoptic pressure gradient and thermal contrast can play important roles (e.g., Liu et al. 2000; Banta et al. 2004; Wagenbrenner et al. 2018). Chrust et al. (2013) reported a strong local nocturnal wind at the exit of a narrow canyon, Weber Canyon (Utah), in the United States. They called this wind a "thermally driven valley-exit jet" to distinguish it from the ordinary gap winds driven by a synoptic pressure gradient.

Hijikawa-Arashi appears to be similar to the wind reported by Chrust et al. (2013), yet differs with respect to the following points. 1) As mentioned above, there is only a weak slope of the valley bottom along the Hijikawa River, so that katabatic downslope acceleration (as is important for nocturnal valley winds; e.g., Whiteman 1990) is negligible. 2) The horizontal thermal contrast across the valley along the Hijikawa River is mainly between the air over the Seto Inland Sea and that in the Ozu basin. This contrast is larger than that between the sea and the coastal area or between the coastal area
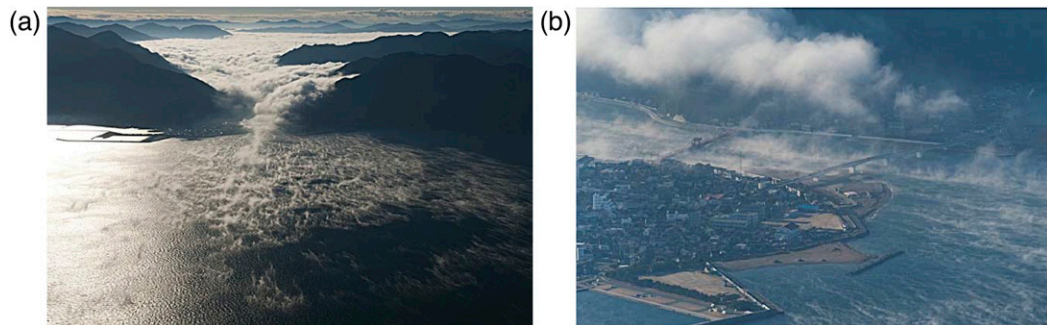


FIG. 2. Airborne photograph of Hijikawa-Arashi. Viewed from the Seto Inland Sea in the (a) northeast and (b) north of the Nagahama estuary on 5 Nov 2014 (courtesy of Ozu City).
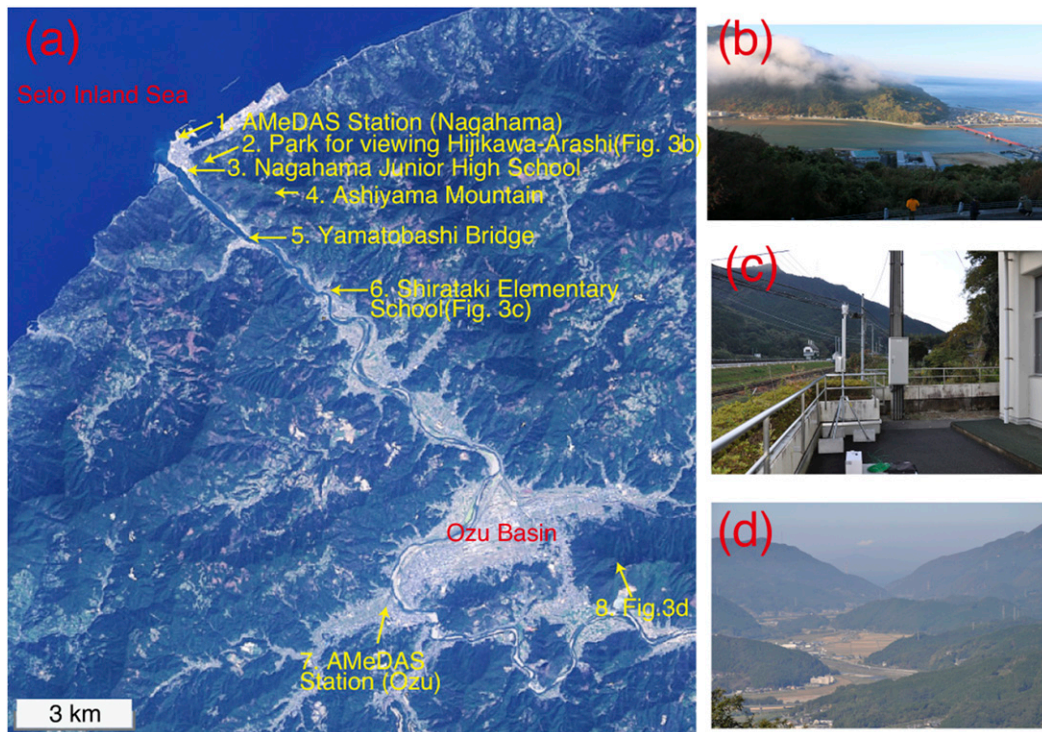
FIG. 3. (a) Satellite image of the region around part of the Hijikawa River and the surface observation sites of the present study: (b) Nagahama Junior High School, indicated by the arrow in (a) (point 3) and (c) Shirataki Elementary School [point 6 in (a)]. (d) View of the valley from the Ozu basin taken from point 8. The image in (a) is from the Geospatial Information Authority of Japan, and its data source is Landsat8 (GSI,TSIC,GEO Grid/AIST) courtesy of the U.S. Geological Survey.

and the basin. 3) The fog may contribute to nocturnal cooling in the Ozu basin, and it might affect the characteristics of the wind in addition to visualizing the wind. 4) As will be shown in the discussion, enhancement of the wind speed of Hijikawa-Arashi is significant not only at the valley exit (estuary), but also at the right downstream of a gap in the middle of the valley. Therefore, we will call Hijikawa-Arashi a ''thermally driven gap wind.''

Ohashi et al. (2015) carried out surface observations along the Hijikawa River and investigated the environmental conditions that favor the occurrence of strong wind at the estuary, whereas Ohashi et al. (2018) conducted observations to investigate thermo-physiological impacts of the cold winds on people. Several other studies of Hijikawa-Arashi have been published in Japanese. For example, Nagoshi (2009) studied the wind in a laboratory experiment using a scale model of the topography of the valley. Numerical studies on Hijikawa-Arashi have been also conducted, using the Cloud Resolving Storm Simulator (CReSS; Tsuboki and Sakakibara 2002) with a horizontal resolution of 300 m, and Nagoshi et al. (2013) successfully reproduced fog in the Ozu basin and the strong local wind at the estuary

for the observed case of 5 January 2010. However, the horizontal resolution of their study was not fine enough to resolve the narrowest part of the valley. These authors attempted to further improve the horizontal resolution, but a numerical instability prevented their calculation. Shigeta (2009) used the Weather Research and Forecasting (WRF) Model to reproduce the intensified near-surface wind at the estuary and discussed its vertical profile.

To reproduce a realistic Hijikawa-Arashi, a numerical model with full physics is required, which includes realistic topography, fog generation, and radiation. In particular, the model needs to employ very fine resolution to resolve the narrow valley along the Hijikawa River, although a relatively small calculation domain may be used since Hijikawa-Arashi occurs under a weak pressure gradient in a moving high.

The present study undertook a numerical simulation of two cases of Hijikawa Arashi using a JMA nonhydrostatic model (Saito et al. 2006). The aim is to reproduce not only the strong wind speed of Hijikawa-Arashi but also the way in which it is visualized by fog and to understand its dynamics. Very high horizontal resolution of 80 m and fine vertical resolution of 5 m

TABLE 1. Configuration of each experiment.

| | Experiment CC | Experiment FC | Experiment FF |
|---|---|---|---|
| Horizontal resolution $dx$ | 400 m | 400 m | 80 m |
| Vertical resolution $dz$ | 40–723 m | 10–159 m | 10–159 m |
| Number of grid points | $750 \times 750 \times 60$ | $750 \times 750 \times 180$ | $1200 \times 1200 \times 180$ |
| Horizontal domain size | 300 km $\times$ 300 km | 300 km $\times$ 300 km | 96 km $\times$ 96 km |
| Model top | 22 509 m | 15 060 m | 15 060 m |
| Initial date (Case J) | 0000 JST[a] 3 Jan | 0000 JST 3 Jan | 0000 JST 4 Jan |
| Initial date (Case N) | 0000 JST 3 Nov | 0000 JST 3 Nov | 0000 JST 4 Nov |
| Time integration | 36 h | 36 h | 12 (8.88)[b] h |
| Time step | 1 s | 1 s | 0.4 s |

[a] JST is +9 h UTC.
[b] For Case J.

near the surface were used to realistically reproduce the phenomena.

The remainder of this paper is organized as follows. Section 2 describes the numerical model and its configuration, the two cases to be simulated, and the surface observations used to verify the simulation results. Section 3 gives an overview of the numerical results at various resolutions, and section 4 compares the numerical results with surface observations. Section 5 discusses resolution dependence, dynamics, and the processes that accumulate moisture to form the fog. Finally, concluding remarks are presented in section 6.

## 2. Experimental design and target cases

### a. Numerical model

The present study uses the Japan Meteorological Agency's Non-Hydrostatic Model (JMA-NHM), which is one of the regional NWP models used for operational forecasts by the JMA (Saito et al. 2006). Like other NWP models, this model considers many physical processes that are relevant to the atmosphere, surface–atmosphere interaction, and soil. The present study employs the Deardorff (1980) turbulence scheme, the Beljaars and Holtslag (1991) surface-layer parameterization, bulk cloud microphysics, and long- and shortwave radiation. Three kinds of experiments were carried out by changing the resolution as follows:

1) Experiment CC with coarse vertical and horizontal resolution,
2) Experiment FC with fine vertical and coarse horizontal resolution, and
3) Experiment FF with fine vertical and horizontal resolution.

The configuration of each experiment is listed in Table 1. There were 3 times as many vertical levels for Experiments FC and FF as for Experiment CC, while the model top height for Experiments FC and FF was lower than

for Experiment CC. Thus, the vertical resolution of the lower layers in Experiments FC and FF was about 4 times as fine as that in Experiment CC.

Initial and boundary conditions of Experiments CC and FC were given by interpolating the Meso Analysis (MANL)[2] provided by the JMA, whereas those of Experiment FF were given by the output of Experiment FC every 5 min. Sea surface temperatures (SSTs) are also given by interpolating the dataset for each day provided by JMA, but their changes are very small.

The computational domain and topography for each experiment are shown in Fig. 4. Terrain-following coordinates (Saito et al. 2006) were used, and the topography and land were generated by smoothing the 50-m mesh map provided by the Geospatial Information Authority of Japan. The maximum gradient of topography in the numerical model was suppressed to 0.5. The valley along the Hijikawa River is so narrow that experiments with the coarser horizontal resolution (Experiments CC and FC) cannot resolve it adequately, and artificial saddles appear in the valley (Fig. 5a). On the other hand, the experiment with the finer horizontal resolution (Experiment FF) is sufficient to resolve the river path even at the narrowest part of the valley. Some grid cells at the river were assigned as water surface in Experiment FF, although the river is imperfectly resolved and thus is discontinuous (Fig. 5b).

### b. Case overview and field observations

The present study investigates two case studies of observed Hijikawa-Arashi: one on 4 January 2015 that is referred to as Case J and the other on 4 November 2015 (Case N; supplemental movie S1). In both cases, the area was covered by synoptic highs, and fine weather is generally expected (Fig. 6). According to data of surface observatories operated by the JMA, the nighttime

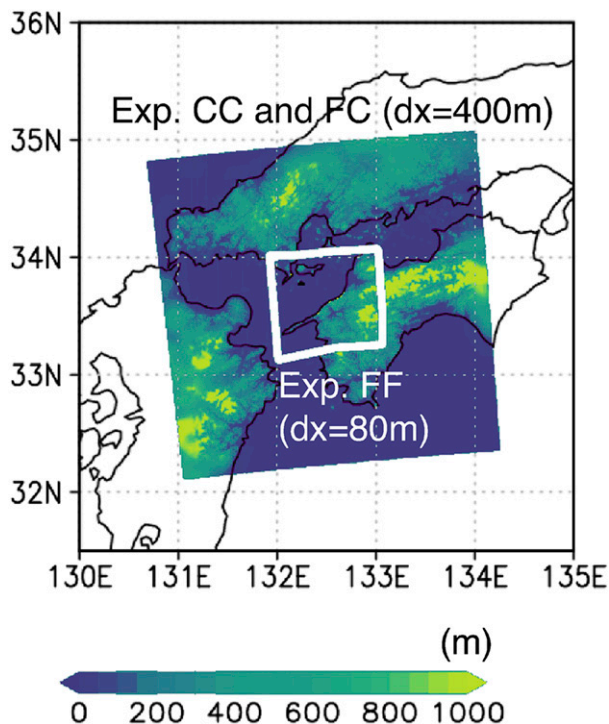[2] MANL is given every 3 h with a horizontal resolution of 5 km.

FIG. 4. Computational domain for Experiments CC and FC (shaded area) and FF (white box). Color shading represents topography.



FIG. 5. Topography in the simulations around the estuary of the Hijikawa River in (a) Experiment FC ($dx = 400$ m) and (b) Experiment FF ($dx = 80$ m). Black lines indicate boundaries between land and water surfaces for each simulation.

weather at Matsuyama observatory (40 km northeast of Ozu) was fair for both cases, and was partially cloudy (Case J) and fair (Case N) in the morning, suggesting that significant radiative cooling occurred during both nights. Similar to the cases described by Ohashi et al. (2015), winds recorded by Automated Meteorological Data Acquisition System (AMeDAS) stations in Ehime prefecture were generally weak northerlies that are less than $5\,\mathrm{m\,s^{-1}}$, except at Nagahama station (point 1 in Fig. 3a), which is located near the estuary of the Hijikawa River.

SSTs were 287 and 294 K for Cases J and N, respectively. In both cases, SSTs were 10 K or more warmer than the lower atmosphere in the basin during the morning. Such a large temperature contrast is characteristic of the cold season.

We made our own observations only for Case N. As referred to in section 1, visual observations were conducted by drone (DJI Phantom2 VISION+). The drone was launched from the top of Ashiyama (point 4 in Fig. 3a) at a height of 482 m, and video footage was recorded at 250 m above ground level (AGL). Anemometers (Vaisala WXT520) and thermometers (TANDD Thermo Recorder TR-73U) were placed at two sites (Figs. 3b,c): on the roof of Nagahama Junior High School at the estuary (Fig. 3b; point 3 in Fig. 3a) at
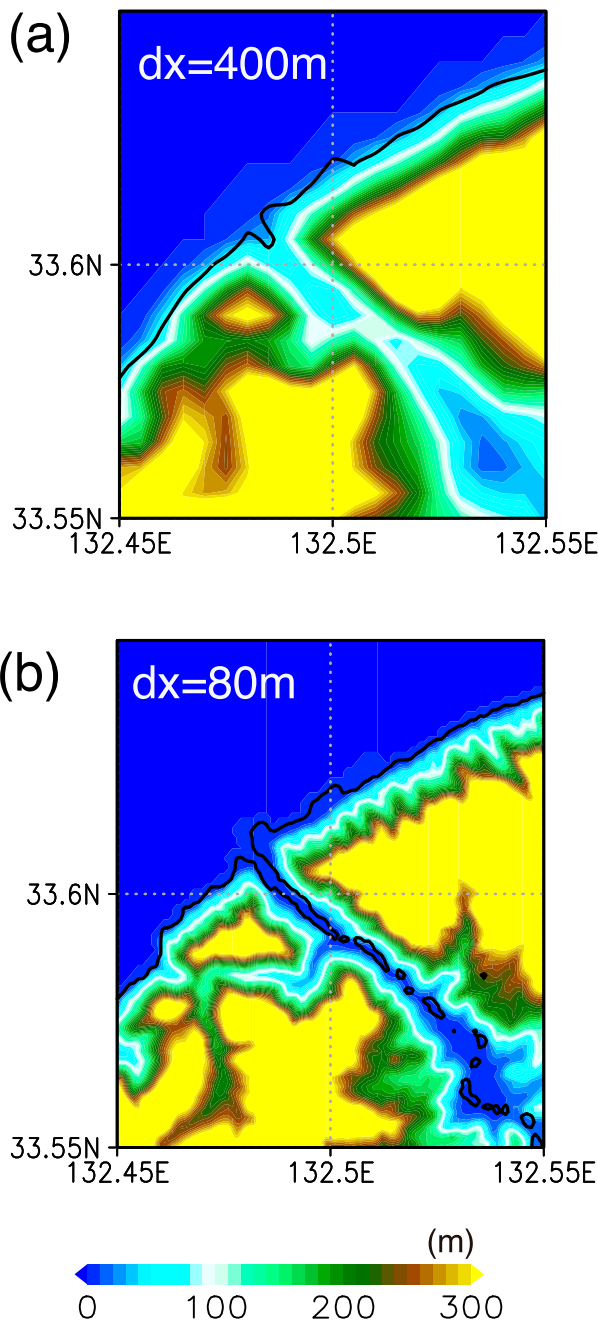
~15 m AGL, and near the ground at Shirataki Elementary School, which is located about 1 km upstream of the narrowest point of the valley (Fig. 3c; point 6 in Fig. 3a). Since these instruments were not deployed in Case J, we use data from AMeDAS stations at Nagahama and at the center of the Ozu basin (point 7 in Fig. 3a) to analyze Case J.
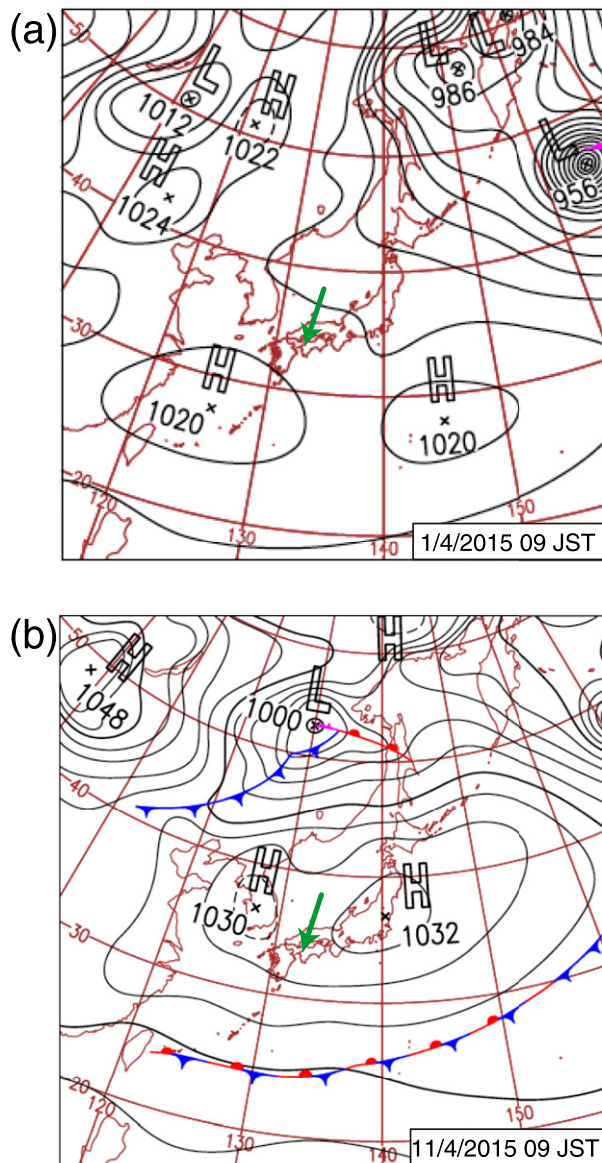
FIG. 6. Surface weather maps for (a) Case J and (b) Case N provided by the JMA. The area where Hijikawa-Arashi occurs is indicated by green arrows.

## 3. Numerical results

In the following, most of the results are for Case J, for which the simulated fog was denser. Figure 7 shows the simulated surface wind speed at 10 m AGL at 0700 Japan standard time (JST) for Case J. Remarkably strong southeasterly winds occurred near the estuary of the Hijikawa River, even in Experiment CC, which has the coarsest resolution. The strong southeasterly wind was confined to the areas around the estuary, as reported by Ohashi et al. (2015); this was also evident in the simulation of Case N (not shown).
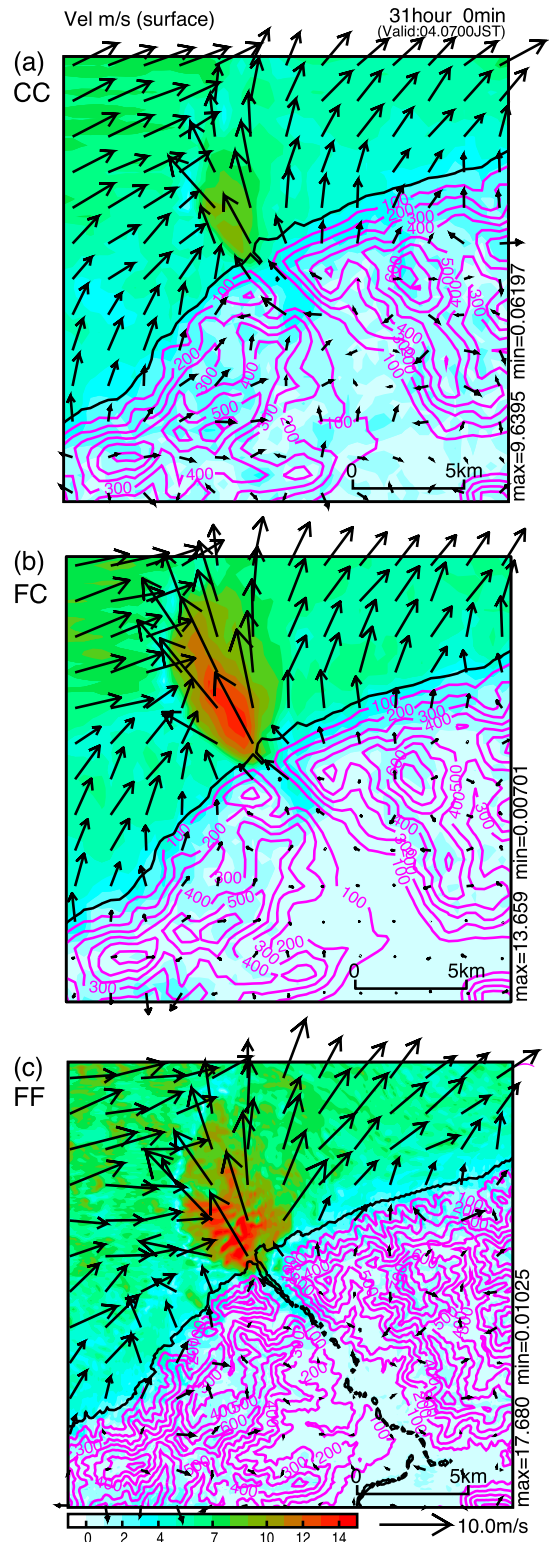


FIG. 7. Surface wind near the estuary. Surface wind vectors (arrows), their magnitude (shading), and topography (purple contours) for Experiments (a) CC, (b) FC, and (c) FF.

Experiments with the finer vertical resolution (Experiments FC and FF) produced stronger along-valley wind than in Experiment CC (Fig. 7), and this stronger wind will be shown to be more reasonable (section 5a). The difference in vertical resolution led to a marked difference in the formation of radiation fog in the Ozu basin during the night. Figure 8 shows the potential temperature, water vapor mixing ratio, and cloud water mixing ratio at the center of the Ozu basin, and Fig. 9 shows the accumulated column-integrated cloud water mixing ratio below 300-m height, which may be regarded as fog. The experiment with the finer vertical resolution (Experiment FC) yielded lower near-surface temperature than Experiment CC, with a temperature difference in the midnight between 25 and 5 m AGL exceeding 5 K (Fig. 8a). The water vapor mixing ratio for Experiment FC was slightly higher than that for Experiment CC (Fig. 8b).

In Experiment FC that started from the previous day, the temporal evolutions of wind and potential temperature profiles at the estuary and in the basin are shown in Fig. 10. In both Case J and Case N, convective boundary layers with northerly or northwesterly sea breezes develop in the daytime on the previous day; in turn, southeasterlies in the shallow layers near the ground corresponding to Hijikawa-Arashi become significant soon after the sunset. Onsets and ends of the southeasterlies are remarkably different between the two cases probably because of the larger-scale environments. In particular, the strong southeasterlies kept flowing after sunrise and did not cease even at 1200 JST in Case J (Fig. 10a). This occurred because upper-layer clouds covering the region intervened the solar radiation to warm up the ground and cold airmass in the Ozu basin.

When the horizontal resolution was also increased (i.e., from Experiments FC to FF), the maximum surface wind speed increased from 13.7 to 17.7 m s$^{-1}$ (Figs. 7b,c). The surface wind speed over the sea exhibited a pattern of stripes parallel to the coastline in Experiment FF (Fig. 7c). A similar stripe pattern, visualized by fog, was actually observed over the sea (Fig. 2a). This pattern may be associated with the gravity wave at the top of the shallow cold flow (Fig. 10a).

The amount of fog in the Ozu basin varied little between Experiments FC and FF (Figs. 9b,c); however, a significant difference is found near the estuary: the fog was blocked by the unrealistic saddle in the valley in Experiment FC (Fig. 9b), whereas it flowed through the valley and reached the sea in Experiment FF (Fig. 9c). A previous simulation using CReSS with a coarser horizontal resolution of 300 m (Nagoshi et al. 2013) gave results similar to those of Experiment FC.

A three-dimensional visualization of simulated cloud water mixing ratio for Experiment FF is shown in Fig. 11,
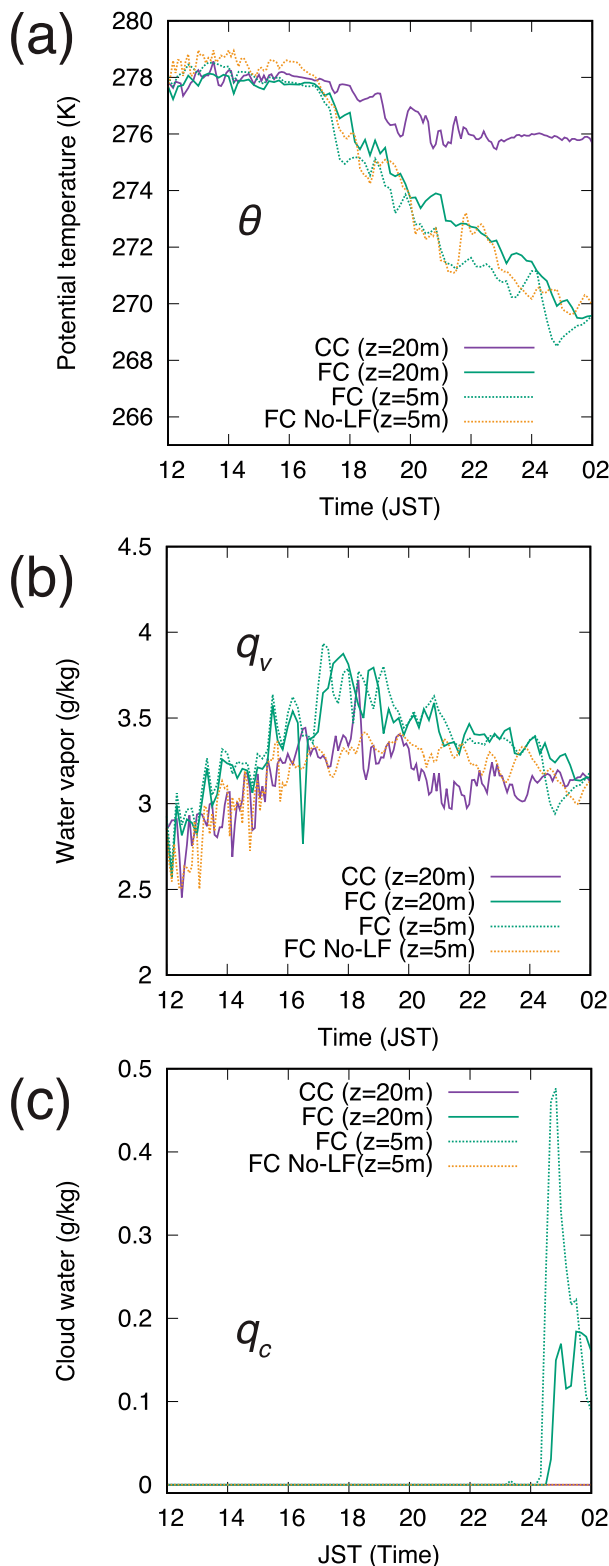


FIG. 8. Time series of (a) potential temperature $\theta$, (b) water vapor $q_v$, and (c) cloud water mixing ratio $q_c$ at heights of 5 and 20 m at the center of the Ozu basin where the AMeDAS station (Ozu) is located (point 8 in Fig. 3a) for various experiments for Case J.
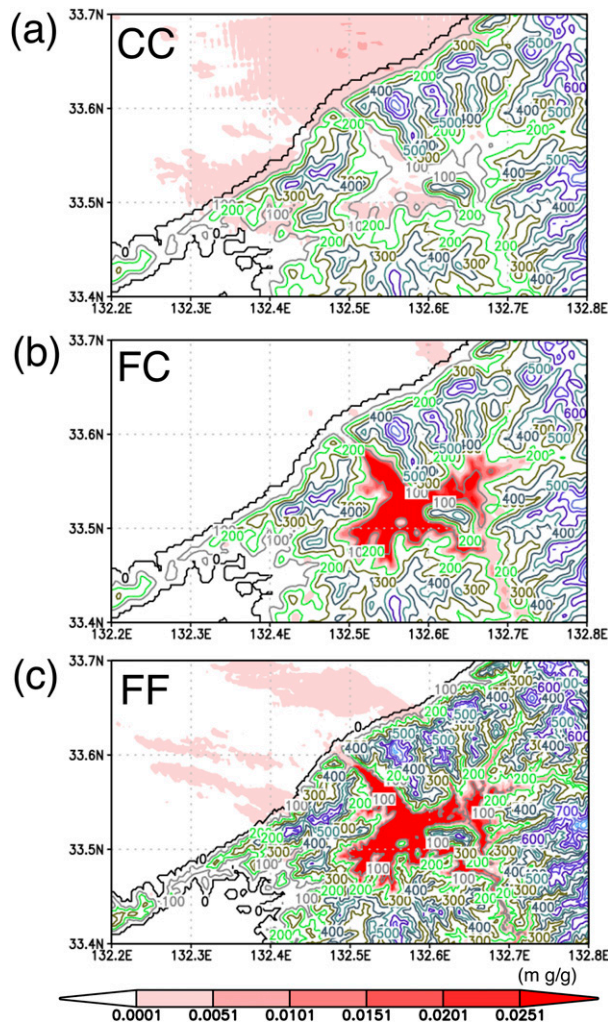
FIG. 9. Column-integrated cloud water mixing ratio below $z = 300$ m (shading) and topography (contours) for Experiments (a) CC, (b) FC, and (c) FF at 0700 JST for Case J.

and an animation of the results is presented in supplemental movie S2. The visual appearance of Hijikawa-Arashi was reproduced well. The fog layer shows a slight eastward deflection near the estuary (Fig. 11b), which is commonly observed in reality (e.g., Fig. 2a).

As mentioned in the previous section, the fog was denser in Case J than in Case N. In fact, the strong wind over the estuary and the fog in the Ozu basin are reproduced in Case N; however, the simulated fog dissipated before reaching the estuary even in Experiment FF.

## 4. Comparison with surface observations

The results of Experiment FF for Case N are now compared with the time series of surface observations recorded at Nagahama Junior High School (point 3 in

Fig. 3). Figure 12a shows reasonable agreement between the simulated and observed horizontal wind speed in terms of the intensity and temporal variations; however, the variance of the simulated wind speed is much smaller, and the average of the simulated wind speed is systematically slightly higher than that observed. The simulated temperature near the surface also agrees reasonably well with the observations, although the former is slightly lower (Fig. 12c). Numerical instabilities developed during the time integration in Case J, soon after 0800 JST in Experiment FF, and the time integration was halted. It was difficult to identify the cause of the instability.

Wind speed and temperature observed at Shirataki Elementary School, which is located upstream of the narrowest part of the valley (point 6 in Fig. 3a), are compared with the simulation results in Figs. 12b and 12d. The simulation results agree reasonably well with the observations; however, the simulated temperature is systematically colder than that observed, and this appears to result in the stronger wind speed at the estuary (Fig. 12a).

## 5. Discussion

### a. Resolution dependence

The results in section 3 suggest that the vertical resolution significantly affects whether fog is formed in the Ozu basin (Figs. 9a,b). The fog started to form around the midnight in Experiment FC (Fig. 8c). A crucial factor in the formation of the fog is the temperature of the lowest level of the atmosphere after sunset (Fig. 8a).

During the daytime smaller differences in the mixing ratio of the water vapor and temperature are found between experiments with different resolutions (Figs. 8a,b). After sunset, however, the temperature at the ground surface, as calculated by the soil model, starts to decrease because of radiative cooling, and the atmospheric temperature at the lowest grid level depends strongly on the vertical resolution (Fig. 13); that is, the atmospheric temperature at the lowest grid level closely follows that of the ground surface for Experiment FC, but not for Experiment CC. Figure 8a also shows that potential temperature $\theta$ at $z = 20$ m, which is the second lowest level in Experiment FC, also decreases in accordance with the temperature at the lowest level. The difference in the lowest level affects the temperature evolution at higher levels. We also tested the surface-layer parameterization of Businger et al. (1971) and found a similar temporal evolution of temperature at the lowest grid level (not shown). These results suggest that the heat capacity of the lowest atmospheric layer decreases when
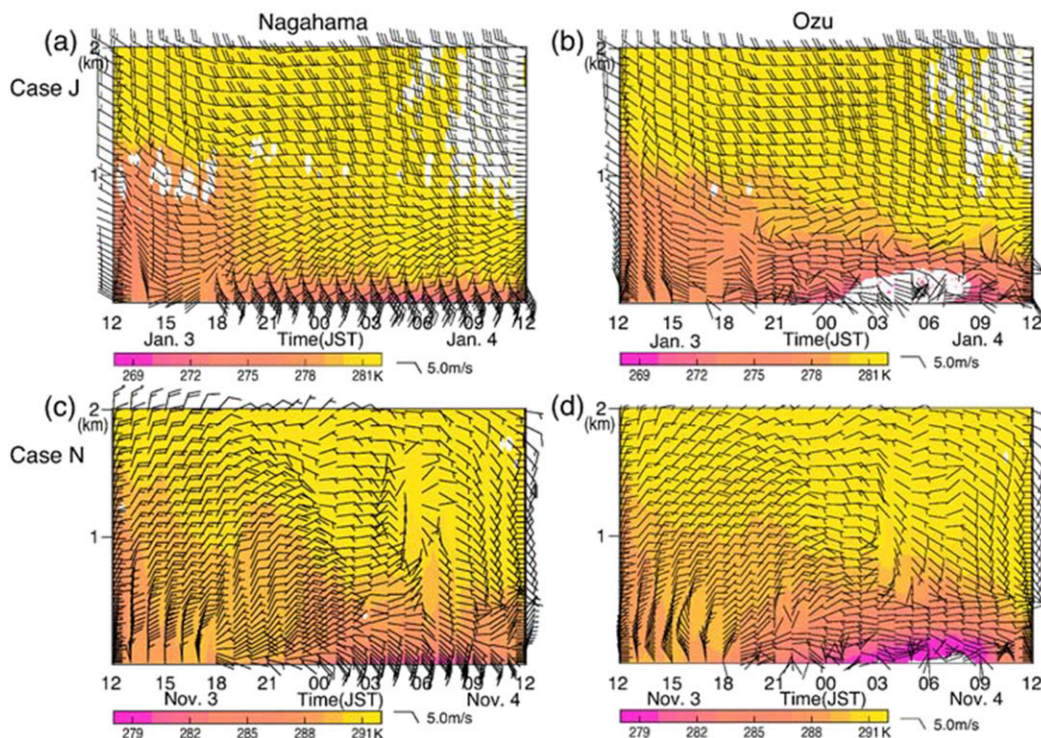
FIG. 10. Potential temperature (shading), the height with cloud water mixing ratio larger than $0.01\,\mathrm{g\,kg^{-1}}$ (white hatching), and horizontal wind speeds (wind barbs) in a time–height cross section (a),(c) at the estuary (Nagahama) and (b),(d) in the basin (Ozu) for (top) Case J and (bottom) Case N in Experiment FC. Note that the ranges of the shading are different between the top and bottom panels.

the vertical grid size is decreased; consequently, given the heat flux at the ground surface, the atmospheric temperature follows more closely that of the ground surface.

The evolution of the radiation fog after its formation seems to be similar to that reported by Nakanishi (2000). The fog at $z = 5\,\mathrm{m}$ appears prior to that at $z = 20\,\mathrm{m}$ (Fig. 8c). Once the fog forms just above the ground, upward longwave radiation from the top of the fog layer causes active convection in the layer and effectively cools the temperature of the whole layer, even in the presence of warming, because of the release of latent heat. After the fog started to develop in Experiment FC at 0000 JST 4 January, the temperature of the lowest atmospheric level actually decreased further by 2 K (Fig. 13). On the other hand, the temperature of the ground started to increase soon after the fog formed, probably because of the downward longwave radiation from the fog.

Although we did not carry out surface observations for Case J, surface temperature data from the AMeDAS station at the center of the Ozu basin are available. The observed time series of surface temperature indeed continued to decrease after sunset (Fig. 13) and is more consistent with the simulated temperature for Experiment FC than for Experiment CC.

We conducted an additional experiment in which only the resolution at the lowest level for Experiment CC is improved from 40 to 10 m while the number of vertical levels is kept at 60. The result of this experiment (not shown) indicates that the fine resolution at the lowest level is particularly important for the fog near the surface.

Figure 14 compares the wind speed and surface temperature at the estuary among Experiments CC, FC, and FF. For both Cases J and N, the wind speed is strongest in Experiment FF. The wind speeds at the estuary are significantly different between Experiments FC and FF, although the temperature differs little (Fig. 14). Two possible reasons for the greater wind speed in Experiment FF may be considered: first, the finer topography can resolve the narrow valley, which is likely to result in a higher wind speed (see the following subsection); second, the bottom boundaries of some grid cells on the Hijikawa River in Experiment FF are classified as water surface, which has weaker friction than land and thus contributes to the higher wind speed (Fig. 5b).

### b. Dynamics

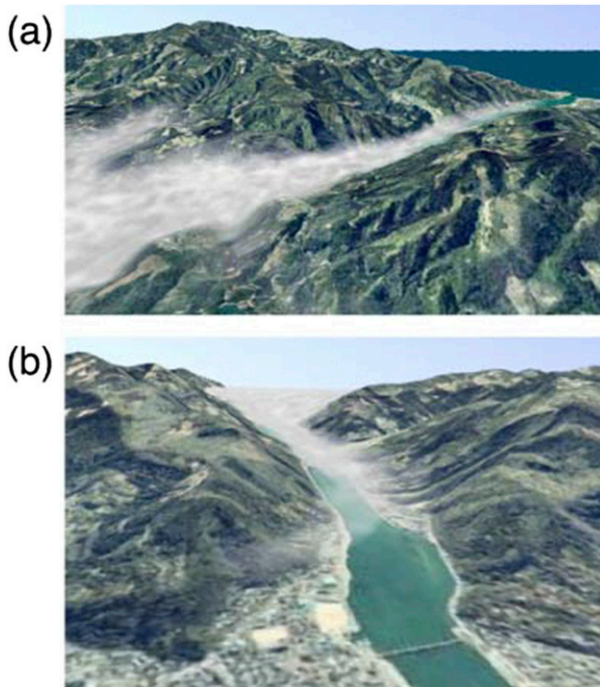As mentioned in section 1, the enhancement of surface wind speed downstream of the narrow valley

FIG. 11. Three-dimensional visualization of the simulated Hijikawa-Arashi for Experiment FF for Case J: (a) looking north, with the estuary at the upper right; (b) looking south from the estuary.

appears to be associated with a supercritical hydraulic flow. The cold air in the basin flows out along the Hijikawa River while it accelerates and reduces its layer thickness (Fig. 15a; the time evolution is shown in Figs. 15d,e, and supplemental movie S3).

The flow depicted in Fig. 15 is not simple. At least two jumps accompanying increases in the layer depth of the cold air appear to occur along the final 5 km of the river. As seen from movie S3, these jumps occur at fixed locations and remain stationary. The first jump occurs downstream of the narrowest point of the valley (J1 in Fig. 15a). Downstream of the narrowest point, the width of the valley increases near Yamatobshi Bridge (point 5 in Fig. 3) where a tributary joins the Hijikawa River. Then another jump occurs at the estuary (J2 in Fig. 15a). Two obvious increases in surface wind speed along the Hijikawa River are indeed found upstream of the jumps (Fig. 15b). Multiple hydraulic jumps over a longer distance have been reported for a gap wind in Howe Sound, British Columbia (Finnigan et al. 1994).

The temperature deficit $\Delta\theta$ of the cold airmass upstream of the narrowest point (point A in Fig. 15d) with respect to the air over the sea is about 12 K, and the thickness of the cold air mass $d$ is about 450 m. This induces a positive hydrostatic pressure anomaly $\Delta p \sim \rho g' d \sim 140$ Pa, where $g' \equiv g(\Delta\theta/\theta_0)$ is the reduced gravity, $g$ is gravitational acceleration, $\theta_0$ is the standard temperature, and $\rho$ is the density of the air. This hydrostatic pressure anomaly is comparable to the difference in the simultaneously observed sea level pressure between the basin and estuary, as reported by Ohashi et al. (2015).

The Froude number ($F_r \equiv u/\sqrt{g'd}$) at point A is estimated as $\sim 0.14$ ($u \sim 2$ m s$^{-1}$), which is subcritical. In the area between the two jumps (e.g., point B in Fig. 15, where $u \sim 11$ m s$^{-1}$ and $d \sim 205$ m), $F_r \sim 1.06$, which is slightly supercritical. At the estuary (point C in Fig. 15, where $u \sim 14$ m s$^{-1}$ and $d \sim 50$ m), $F_r \sim 3.16$, which is supercritical.

Since a clear capping inversion exists above the cold air (Fig. 15d), it is of interest to apply a theoretical analysis of a two-layer flow, which is analogous to shallow water theory. Saito (1992) studied shallow water flow over a saddle-shaped topography and reported a regime with a stationary hydraulic jump. Following Saito (1992), we seek a solution for a stationary hydrostatic jump in a two-layer flow over a channel, although Hijikawa-Arashi in reality is much more complex than assumed in the theory (e.g., multiple jumps as mentioned above, surface friction, and a V-shaped valley as seen in Fig. 3d). Using the notation of Saito (1992), the system of governing equations may be written as follows:

$$\frac{u_i^2}{2g'} + h_i = \frac{u_-^2}{2g'} + h_-, \tag{1}$$

$$\frac{u_d^2}{2g'} + h_d = \frac{u_+^2}{2g'} + h_+, \tag{2}$$

$$h_i u_i b_0 = h_- u_- b_j = h_+ u_+ b_j = h_d u_d b_0, \quad \text{and} \tag{3}$$

$$u_- = \sqrt{\frac{h_+}{h_-} g' \frac{h_- + h_+}{2}}, \tag{4}$$

where $h_i$ and $u_i$ are the height and velocity of the cold air upstream of the narrow part, respectively; $h_-$ and $u_-$ are those upstream of a jump, and $h_+$ and $u_+$ are those downstream of a jump; $h_d$ and $u_d$ are those far downstream; and $b_o$ and $b_j$ are channel widths upstream and at the jump, respectively. After nondimensionalization, the above system for 6 equations with 10 unknowns is shown to be governed by two nondimensional numbers (Buckingham $\pi$ theorem): the Froude number $F_r \equiv u_i/\sqrt{g'h_i}$ in the far upstream and the ratio of the channel width at the jump to upstream $B_j \equiv b_j/b_0$. The solution also must satisfy the critical condition $1 + 0.5F_r^2 - 1.5(F_r/B_j)^{(2/3)} \le 0$ (Long 1953).

Figure 16 shows the enhanced wind speed upstream of the jump $u_-/u_0$ over the parameter space of $F_r$ and $B_j$.
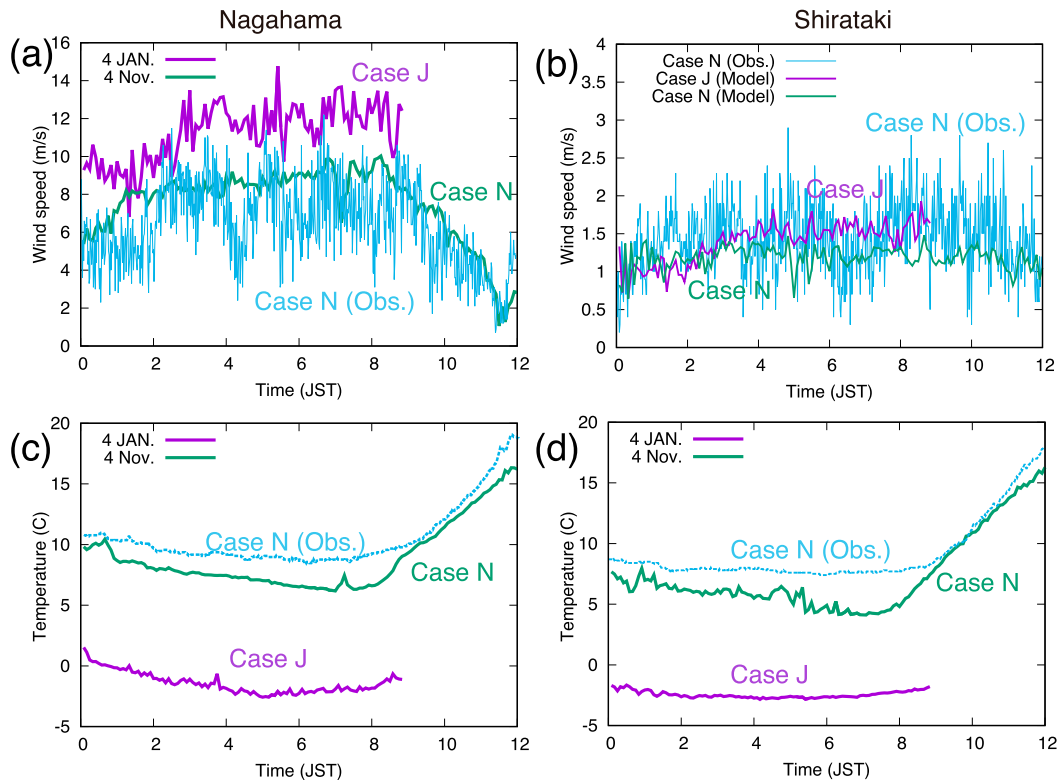
FIG. 12. (a),(b) Wind speed and (c),(d) temperature observed at (left) Nagahama Junior High School and (right) Shirataki Elementary School (light blue) for Case N and the results of Experiment FF at the closest grid point to the school at a height of 15 m for Cases J (purple) and N (green). The time interval of the observation date is 1 min, while those of the model outputs are 5 min.

This result shows that smaller $F_r$ and $B_j$ result in stronger enhancement of the wind speed downstream of the jump. Upstream of the narrower part of the valley, $F_r \sim 0.14$, as estimated above. Since the real valley has a V-shaped cross section (Fig. 3d), it is difficult to estimate an appropriate $B_j$. However, if a typical valley width and the basin scale are assumed to be 500 m and 5 km, respectively, $B_j$ is about 0.1. Thus, Fig. 16 suggests that a significant enhancement of the wind speed (~10 times) is expected.

Now we examine whether the presence of fog affects the dynamics. To investigate the contribution of the fog, we conducted a sensitivity experiment for Case J (Experiment FC-Dry) in which the condensation of water vapor is turned off, but is otherwise configured as in Experiment FC. The results of Experiment FC-Dry suggest that the wind was almost as strong at the estuary as in Experiment FC, even in the absence of fog (Fig. 14a). The temperature at the estuary also differed little (Fig. 14c). Radiative cooling from the top of the fog (partly compensated by latent heating due to the condensation of fog) in Experiment FC is likely to be comparable to that from the ground to the open sky in

Experiment FC-Dry. In Experiment FC-Dry, the mixed layer owing to the radiative cooling at the top (Point A in Fig. 15e) is not formed in the basin, and the surface temperature is about 3 K colder than in Experiment FC. Despite the difference in vertical profiles of $\theta$, the pressure anomaly at the surface, $\Delta p \sim \int_0^d \rho g' \, dz$, is similar in the two runs. This result may be fortuitous for the present Case J; however, it suggests that the fog is not essential to intensifying the wind speed, although it is crucially important for visualizing Hijikawa-Arashi.

*c. Water vapor supply*

The water vapor in the basin, which is the source of the fog during the night, continues to increase during the daytime and after sunset (Fig. 8b). One possible source is evaporation from the land surface. Another possible source of water vapor in the basin is advection by the sea breeze during the daytime. In fact, the wind direction at the estuary in the afternoon of the previous days is opposite to that of Hijikawa-Arashi (Fig. 10).

A sensitivity experiment was undertaken to examine the contribution of the former (Experiment FC-NoLF), employing the same configuration as Experiment
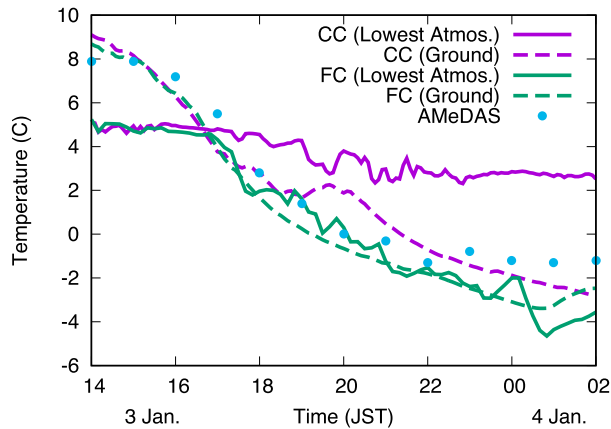
FIG. 13. Time series of atmospheric temperature at the lowest grid level (solid lines) and the ground surface temperature (dashed lines) for Experiments CC (purple) and FC (green) for Case J at the center of the Ozu basin. Hourly data recorded at the AMeDAS station (Ozu) are shown by light blue dots.

FC except that the soil water is set to zero throughout the time integration. The NWP model prescribes the surface water vapor flux from the land to the atmosphere by considering the soil water budget. Therefore, the surface water vapor fluxes from the land only are eliminated.

As a result of reduced vapor supply from the land, the amount of cloud water corresponding to the fog in the lower atmosphere in Case J is significantly decreased (Figs. 9b and 17). Nevertheless, the wind speed and temperature at the estuary vary little between Experiment FC and Experiment FC-NoLF (Figs. 14a,c), which is consistent with the results of Experiment FC-Dry.

Figure 8b shows that the water vapor mixing ratio in the basin in Experiment FC-NoLF increases in almost the same manner as in Experiment FC during the daytime, and this suggests that advection by sea breezes is also important. Furthermore, the difference between Experiments FC and FC-NoLF becomes larger after sunset (after 1600 JST in Fig. 8b). Nocturnal katabatic valley winds (e.g., Whiteman 1990) from various valleys converge at the center of the basin, and contribute to the accumulation of water vapor. In Experiment FC-NoLF, the katabatic winds are drier because of the absence of the water vapor flux from the land surface.

Another sensitivity experiment was conducted (Experiment FC-NoSea), employing the same configuration as Experiment FC except that the sea surface in a square of about 100 km × 100 km around the estuary of the Hijikawa River is changed to the land (Fig. 18a). As a result, the cloud water in the basin in the next morning almost disappears in Experiment FC-NoSea (Fig. 18b).
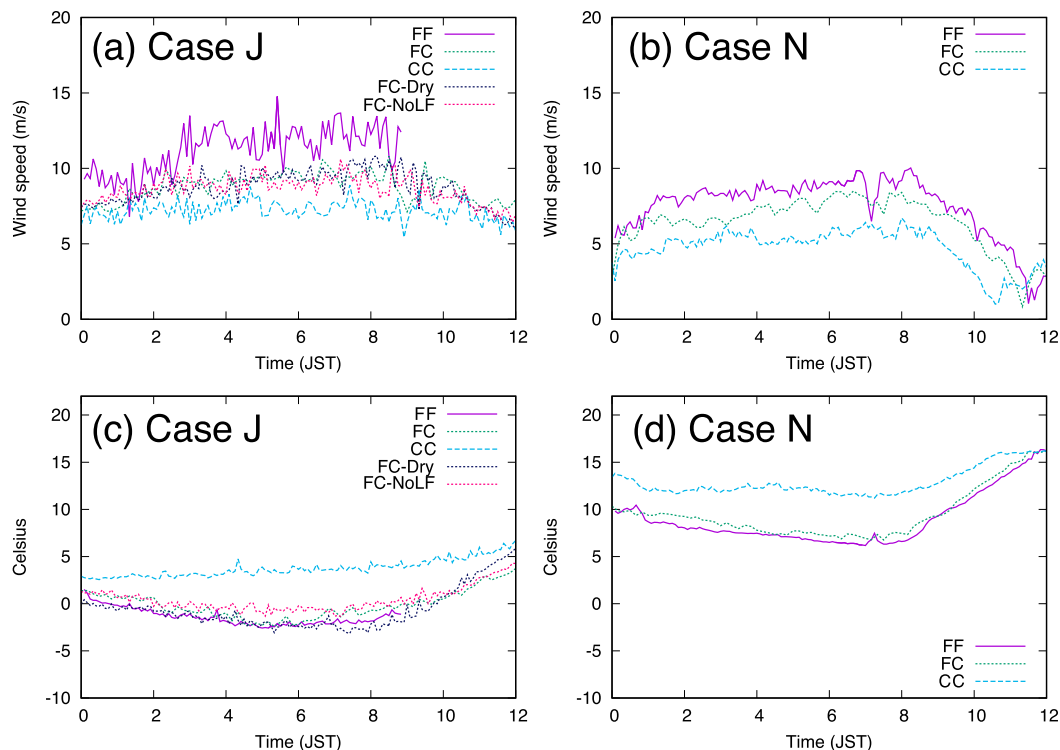


FIG. 14. (a),(b) Wind speed and (c),(d) temperature observed at Nagahama Junior High School (estuary) for (left) Case J and (right) Case N for various configurations of numerical experiments.
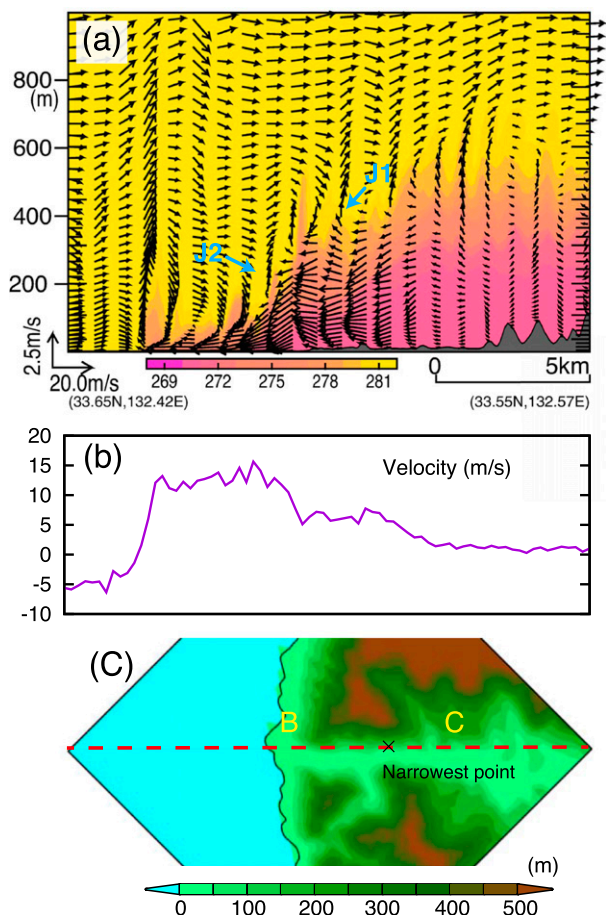
FIG. 15. (a) Potential temperature (shading) and wind vectors, and (b) horizontal wind velocity at 10 m AGL (positive to the left) along the red dotted line shown in (c) that shows topography by shading. The locations of two jumps are indicated as J1 and J2 in (a). The narrowest point in the valley is marked by the cross in (c), and vertical profiles of potential temperature and horizontal velocity, at points A, B, and C in (c), are shown in (d) and (e), respectively.

This result confirms the daytime sea breeze substantially contributes to the water vapor supply.

*d. Enhanced thermal contrast*

This subsection clarifies that the sea has another role in addition to the water vapor supply. The configuration of Experiment FC-NoSea exhibited in the previous subsection is similar to other thermally driven gap winds for which a small basin is connected to a larger basin through a narrow valley. Now, the ground surface temperature decreases in the night because of radiative cooling on the drained land in Experiment FC-NoSea. The ground surface temperature in the basin is about 270 K in the morning of Case J, and SST of the Seto Inland Sea is almost fixed to be 287 K. Whereas, in Experiment FC-NoSea, that of the drained land is 277 K.
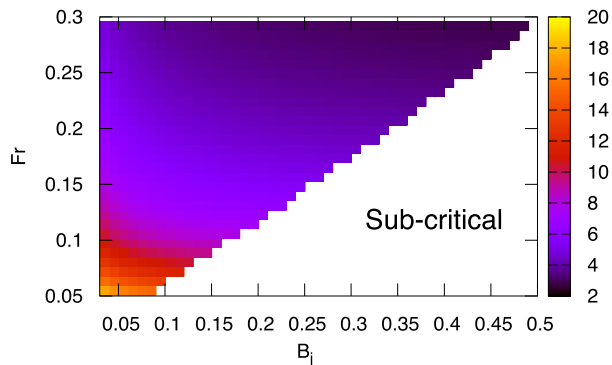


FIG. 16. Enhancement of flow speed upstream of a hydraulic jump $u_-/u_0$ over the parameter space of the Froude number $F_r$ and the ratio of the channel width at the jump to upstream $B_j$ predicted by the analytic solution of a two-layer flow.

Figure 18c shows surface wind speed around the estuary of the Hijikawa River in Experiment FC-NoSea. The gap wind indeed occurs by virtue of the characteristic topography. However, compared with Experiment FC (Fig. 7b), the surface wind speed associated with the gap wind is about $2\,m\,s^{-1}$ weaker. This deceleration appears to be caused by the smaller thermal contrast in the absence of the sea. These results show that Hijikawa-Arashi is driven by the horizontal gradient of hydrostatic pressure between the Ozu basin and the Seto Inland Sea. The pressure tends to be higher in the Ozu basin where the downslope winds along the radiatively cooled surrounding slopes and compensating adiabatic ascents in the center accumulate cold air effectively. The warm air caused by the SST over the sea also contributes to increase the horizontal pressure gradient.

## 6. Conclusions

Hijikawa-Arashi, a thermally driven gap wind that occurs in the northwestern part of Shikoku Island in Japan during the cold season, was reproduced reasonably well by a NWP model with fine horizontal (80 m) and vertical resolution (∼10 m near the surface). Although it is not usual to employ such a fine resolution in a NWP model, the present study demonstrated its potential in simulating microscale meteorological phenomena. Simulated temporal variations in temperature and wind speed agree reasonably well with those observed at surface stations. Even the fog layer flowing out over the Seto Inland Sea from the estuary, which is one of the unique features of Hijikawa-Arashi, is reproduced for one case.

Fine vertical resolution near the surface is essential in simulating a realistic cooling of the lower atmosphere after sunset and fog formation in the Ozu basin.
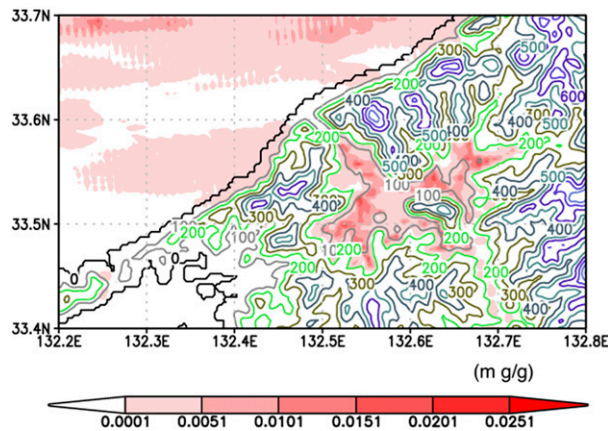
FIG. 17. As in Fig. 9b, but for Experiment FC-NoLF in which soil water is eliminated.

At coarse vertical resolution, the temperature of the lower atmosphere is less affected by that of the land surface. This issue is likely to commonly arise when nocturnal stable boundary layers are simulated in NWP models.

The successful numerical simulation clarifies the dynamics and environmental features of Hijikawa-Arashi. The temperature contrast of 10 K or more between the air over the sea and that in the Ozu basin develops because of nighttime radiative cooling of the land. The strong wind at the estuary is caused by the outflow of cold air that accumulated over the Ozu basin and is enhanced by the narrow gap in the valley of the Hijikawa River. Detailed features of Hijikawa-Arashi were also simulated well; for example, two distinct hydraulic jumps occur, one just downstream of the narrowest part of the valley and the other at the estuary; and the river surface with relatively low surface friction helps to form the strong wind.

Water vapor provided by the daytime sea breeze and evaporation from the land surface seem to be important in forming the fog in the Ozu basin. Although the fog is important for visualizing the wind, it may not be critical to the dynamics. The wind of the same strength can occur in an environment with less water vapor supplies owing to the characteristic topography.

The present resolution may be insufficient to simulate steam fog observed on the surface of water bodies (e.g., Fig. 2b) and that takes the form of longitudinal rolls, which is a preferred pattern of thermal convection in the presence of a strong vertical shear (Asai 1970). An additional issue concerning steam fog is the temperature of the water surface, as no high-resolution data of sea surface temperature in the Seto Inland Sea were available for the present simulation. Furthermore, no data were available for the river surface temperature, so that we tentatively employed the SST of the nearby sea in its place.
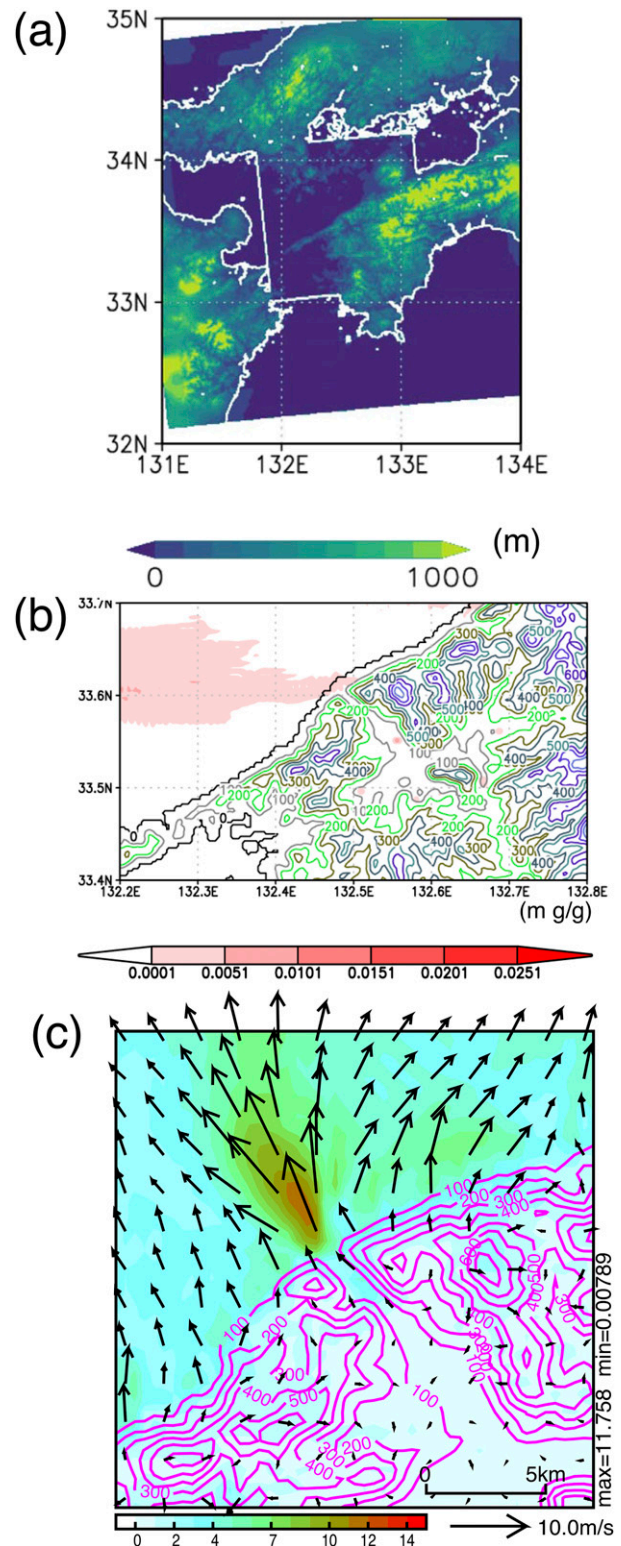


FIG. 18. (a) Topography and coast lines (white), (b) column-integrated cloud water mixing ratio below $z = 300$ m (shading) as in Fig. 9, and (c) surface wind vectors (arrows) and magnitude (shading) as in Fig. 7 in Experiment FC-NoSea.

The enhancement of the wind at the estuary is relatively easy to predict with a NWP model. In fact, it was even reproduced in Experiment CC when no fog was formed for Case J. Since Hijikawa-Arashi visualized by fog is an important tourist attraction, its prediction may be useful for tourists. We have shown that finer horizontal and vertical resolutions, realistic topography, and details of land use are necessary for its accurate prediction. Furthermore, reliable representation of turbulent diffusion seems to be important in predicting whether the fog is advected to the estuary or dissipated along its path. This remains a topic to be studied in the future.

REFERENCES

Asai, T., 1970: Stability of a plane parallel flow with variable vertical shear and unstable stratification. *J. Meteor. Soc. Japan*, **48**, 129–139, https://doi.org/10.2151/jmsj1965.48.2_129.

Banta, R. M., L. S. Darby, J. D. Fast, J. O. Pinto, C. D. Whiteman, W. J. Shaw, and B. W. Orr, 2004: Nocturnal low-level jet in a mountain basin complex. Part I: Evolution and effects on local flows. *J. Appl. Meteor.*, **43**, 1348–1365, https://doi.org/10.1175/JAM2142.1.

Beljaars, A. C. M., and A. A. M. Holtslag, 1991: Flux parameterization over land surfaces for atmospheric models. *J. Appl. Meteor.*, **30**, 327–341, https://doi.org/10.1175/1520-0450(1991)030<0327:FPOLSF>2.0.CO;2.

Businger, J. A., J. C. Wyngaard, Y. Izumi, and E. F. Bradley, 1971: Flux-profile relationships in the atmospheric surface layer. *J. Atmos. Sci.*, **28**, 181–189, https://doi.org/10.1175/1520-0469(1971)028<0181:FPRITA>2.0.CO;2.

Chrust, M. F., C. D. Whiteman, and S. W. Hoch, 2013: Observations of thermally driven wind jets at the exit of Weber Canyon, Utah. *J. Appl. Meteor. Climatol.*, **52**, 1187–1200, https://doi.org/10.1175/JAMC-D-12-0221.1.

Deardorff, J. W., 1980: Stratocumulus-capped mixed layers derived from a three-dimensional model. *Bound.-Layer Meteor.*, **18**, 495–527, https://doi.org/10.1007/BF00119502.

Finn, D., and Coauthors, 2016: Evidence for gap flows in the Birch Creek Valley, Idaho. *J. Atmos. Sci.*, **73**, 4873–4894, https://doi.org/10.1175/JAS-D-16-0052.1.

Finnigan, T. D., J. A. Vine, P. L. Jackson, S. E. Allen, G. A. Lawrence, and D. G. Steyn, 1994: Hydraulic physical modeling

and observations of a severe gap wind. *Mon. Wea. Rev.*, **122**, 2677–2687, https://doi.org/10.1175/1520-0493(1994)122<2677:HPMAOO>2.0.CO;2.

Liu, M., D. L. Westphal, T. R. Holt, Q. Xu, M. Liu, D. L. Westphal, T. R. Holt, and Q. Xu, 2000: Numerical simulation of a low-level jet over complex terrain in southern Iran. *Mon. Wea. Rev.*, **128**, 1309–1327, https://doi.org/10.1175/1520-0493(2000)128<1309:NSOALL>2.0.CO;2.

Long, R. R., 1953: Some aspects of the flow of stratified fluids: I. A theoretical investigation. *Tellus*, **5**, 42–58, https://doi.org/10.3402/tellusa.v5i1.8563.

Mayr, G. J., and Coauthors, 2007: Gap flows: Results from the Mesoscale Alpine Programme. *Quart. J. Roy. Meteor. Soc.*, **133**, 881–896, https://doi.org/10.1002/qj.66.

Nagoshi, T., 2009: Teaching materials on a fluid experiment of the local wind by using a solid relief model of geographical features: A case study of Hijikawa Arashi, a kind of land breeze with fogs. *Educ. Earth Sci.*, **62**, 65–76.

——, S. Saito, S. Inoue, M. Yoshioka, M. Kato, and K. Tsuboki, 2013: Numerical simulation of fog in "Hijikawa-Arashi" using a cloud resolving model "DVD-CReSS" (in Japanese). *Proc. Meteorological Society of Japan Autumn Meeting*, Sendai, Japan, Meteorological Society of Japan, D117.

Nakanishi, M., 2000: Large-eddy simulation of radiation fog. *Bound.-Layer Meteor.*, **94**, 461–493, https://doi.org/10.1023/A:1002490423389.

Ohashi, Y., T. Terao, Y. Shigeta, and T. Ohsawa, 2015: In situ observational research of the gap wind "Hijikawa-arashi" in Japan. *Meteor. Atmos. Phys.*, **127**, 33–48, https://doi.org/10.1007/s00703-014-0345-1.

——, T. Katsuta, H. Tani, T. Okabayashi, S. Miyahara, and R. Miyashita, 2018: Human cold stress of strong local-wind "Hijikawa-arashi" in Japan, based on the UTCI index and thermo-physiological responses. *Int. J. Biometeor.*, **62**, 1241–1250, https://doi.org/10.1007/s00484-018-1529-z.

Saito, K., 1992: Shallow water flow having a lee hydraulic jump over a mountain range in a channel of variable width. *J. Meteor. Soc. Japan*, **70**, 775–782, https://doi.org/10.2151/jmsj1965.70.3_775.

——, and Coauthors, 2006: The operational JMA nonhydrostatic mesoscale model. *Mon. Wea. Rev.*, **134**, 1266–1298, https://doi.org/10.1175/MWR3120.1.

Shigeta, Y., 2009: Numerical simulation and observation of Hijikawa-arashi. *Proc. Meteorological Society of Japan Autumn Meeting*, Vol. 96, Fukuoka, Japan, Meteorological Society of Japan, D306, http://ci.nii.ac.jp/naid/110007626680/.

Tsuboki, K., and A. Sakakibara, 2002: Large-scale parallel computing of cloud resolving storm simulator. *High Performance Computing: ISHPC 2002*, H. P. Zima et al., Eds., Lecture Notes in Computer Science, Vol 2327, Springer, 243–259.

Wagenbrenner, N., J. Forthofer, C. Gibson, A. Indreland, B. Lamb, and B. Butler, 2018: Observations and predictability of gap winds in the Salmon River Canyon of central Idaho, USA. *Atmosphere*, **9**, 45, https://doi.org/10.3390/atmos9020045.

Whiteman, C. D., 1990: Observations of thermally developed wind systems in mountainous terrain. *Atmospheric Processes over Complex Terrain*, W. Blumen, Ed., Amer. Meteor. Soc., 5–42.

Zängl, G., 2004: A reexamination of the valley wind system in the Alpine Inn Valley with numerical simulations. *Meteor. Atmos. Phys.*, **87**, 241–256, https://doi.org/10.1007/s00703-003-0056-5.